

Revision 1

1

2

3

Phosphoran olivine overgrowths:

4

Implications for multiple impacts to the Main Group pallasite parent body

5

6

Neva A. Fowler-Gerace^{1*} and Kimberly T. Tait^{1,2}

7

8 ¹Department of Earth Sciences, University of Toronto, 22 Russell St., Toronto, ON M5S 3B1,

9 Canada

10 ²Department of Natural History, Mineralogy, Royal Ontario Museum, 100 Queens Park,

11 Toronto, ON M5S 2C6, Canada

12

13

14

15

16

17 *neva.fowler.gerace@mail.utoronto.ca

18

Revision 1

19

Abstract

20 Phosphoran olivine (1-7 wt% P₂O₅) is a metastable phase known from fewer than a dozen
21 meteoritic or terrestrial occurrences. We have thoroughly examined phosphoran olivine in the
22 Springwater pallasite to characterize its distribution, textural relationships, and geochemistry.
23 Phosphoran olivine is abundant in Springwater as randomly distributed millimeter-scale partial
24 overgrowths on the P-free olivine crystals. Geochemical analyses support the substitution
25 mechanism of P into the tetrahedral Si site with octahedral site vacancies for charge balance;
26 observed trace element variations, on the other hand, are not related to P substitution. Element
27 mapping reveals fine-scale oscillatory P zoning in unusual serrate patterns, indicating rapid
28 crystal nucleation from a melt as proposed by Boesenberg and Hewins (2010) and a subsequently
29 variable rate of crystallization. The timing of phosphoran olivine formation in Springwater is
30 constrained to after the period of macroscopic olivine rounding but before the cooling of the
31 metal matrix; because the phosphoran overgrowths overprint specific host grain boundary
32 modifications, we suggest that the episode of extremely rapid cooling necessary to crystallize
33 and preserve this rare phase may have been triggered by an additional impact to the parent body.

34

35 **Keywords:** ANALYSIS, CHEMICAL (MINERAL): phosphoran olivine, CRYSTAL
36 GROWTH: phosphoran olivine, METEORITE: Springwater pallasite, PETROGRAPHY:
37 Springwater pallasite

38

Revision 1

39

Introduction

40 Terrestrial igneous olivine typically contains <0.01-0.04 wt% P₂O₅ (Milman-Barris et al. 2008);
41 occasionally, however, the phase can host orders of magnitude more phosphorus. Olivine
42 containing 1-7 wt% P₂O₅ – generally termed “phosphoran olivine” (e.g. Boesenberg and Hewins
43 2010) – is known from nearly a dozen separate occurrences (Buseck 1977; Buseck and Clark
44 1984; Goodrich 1984; Agrell et al. 1998; Wasson et al. 1999; Goodrich 2003; Tropper et al.
45 2004; Boesenberg 2006; Wang et al. 2007), all but four of which (Goodrich 1984; Agrell et al.
46 1998; Tropper et al. 2004; Boesenberg 2006) are extraterrestrial. Up to 32 wt% P₂O₅ has been
47 reported in olivine from secondary melt inclusions in the Brahin pallasite meteorite (Sonzogni et
48 al. 2009).

49 Because the olivine/melt partition coefficient for P is only 0.001-0.1 (Anderson and Greenland
50 1969; Brunet and Chazot 2001; Boesenberg and Hewins 2010), the presence of several wt%
51 P₂O₅ in olivine suggests extenuating circumstances. Boesenberg and Hewins (2010) have
52 experimentally determined that under rapid crystallization regimes P behaves as if it is
53 compatible in olivine, producing a metastable phosphoran olivine phase that will persist only if
54 cooling below the solidus occurs within several weeks. Olivine may accommodate significant
55 amounts of P through substitution of P⁵⁺ for Si⁴⁺ in the tetrahedral site while Mg²⁺ and Fe²⁺
56 vacancies in the octahedral site balance charge (Buseck and Clark 1984; Boesenberg and Hewins
57 2010). Substitutions involving Li⁺ and Na⁺ (Mallmann et al. 2009) or trivalent cations (Milman-
58 Barris et al. 2008) have been shown to facilitate P incorporation into olivine at trace levels;
59 however, the latter mechanism may not operate in even low-P pallasite olivine given a lack of
60 definitive correlations between P and Cr, Al, Ti, V, Sc, or Ga in the Brenham and Brahin
61 pallasites (McKibbin et al. 2013).

Revision 1

62 It is not known whether rapid crystallization is the only atypical condition required to form
63 phosphoran olivine. The experimental data suggest it can crystallize under the same temperature,
64 composition, and oxygen fugacity parameters as nominally P-free olivine (Boesenberg and
65 Hewins 2010). Still, phosphoran olivine is extremely rare in nature, with five of its reported
66 occurrences in the considerably unusual phase assemblage of pallasite meteorites: primarily large
67 forsteritic olivine grains suspended within an iron-nickel matrix, with accessory phosphates,
68 troilite (FeS), schreibersite ((Fe,Ni)₃P), and chromite. Some workers have suggested pallasitic
69 phosphoran olivine formed below its solidus, following oxidation of P from the schreibersite and
70 metal phases during cooling (Olsen and Fredricksson 1966) and potentially involving
71 replacement of olivine rims by reaction with adjacent phosphates (Buseck 1977). However, it has
72 been noted more recently that a subsolidus origin of pallasitic phosphoran olivine is unlikely
73 given the lack of diffusion profiles within the adjacent metal or P-free olivine; crystallization
74 from a quickly cooling melt as has been achieved experimentally is therefore the most viable
75 mechanism (Boesenberg and Hewins 2010). This cooling rate prerequisite for phosphoran
76 olivine formation is challenging to reconcile with the general assumption that pallasites formed
77 substantially below the surface of their parent body (e.g. Buseck 1977; Scott 1977; Tarduno et al.
78 2012; Boesenberg et al. 2012) and contain evidence within their metal matrices for cooling rates
79 as low as several degrees per million years (Yang et al. 2010).

80 Here we perform a thorough characterization of phosphoran olivine within the Springwater
81 pallasite, a 52.8-kg sample initially recovered in 1931 near Saskatoon, Saskatchewan, Canada.
82 Like three of the other four pallasites known to bear phosphoran olivine, Springwater contains
83 macroscopically rounded olivine grains, a texture thought to arise through the
84 thermodynamically favored reduction in olivine surface area during prolonged contact with the

Revision 1

85 metal matrix at elevated temperatures (Scott 1977; Ohtani 1983; Saiki et al. 2003). This and
86 other textural modifications to Springwater olivine place additional constraints on the prevailing
87 conditions during phosphoran olivine formation and its timing relative to other events in the
88 meteorite's history. In order to refine our understanding of the crystallization mechanisms, we
89 have analyzed major, minor, and trace elements with particular focus on zoning patterns. We
90 complement the geochemical data with detailed observations of the large-scale distribution and
91 textural features of phosphoran olivine in Springwater in order to elucidate the origin of this
92 unusual phase within the Main Group pallasite parent body.

93

94

Methods

95 Three approximately 3 x 5 cm polished thick sections from the Springwater pallasite were
96 examined thoroughly for phosphoran olivine. The P content of this phase is sufficiently high that
97 it can be located using a backscattered electron image with exaggerated contrast. Two of the
98 samples were searched systematically for phosphoran olivine using the JEOL JXA-8230 electron
99 microprobe (EMP) at Queen's University, Kingston, Ontario, using an accelerating voltage of 15
100 kV, a 30 nA beam current, and a focused ≤ 1 μm beam. Individual occurrences were imaged and
101 analyzed for P, Si, Ti, Al, Cr, V, Ca, Fe, Co, Mg, Mn, Ni, K, and Na. Matrix corrections were
102 PAP (Pouchou and Pichoir 1985 - double parabolic $\phi(\rho z)$ function) and the mass absorptions
103 coefficients database was MAC30 (Heinrich 1986). Additional points were analyzed for P, Si,
104 Fe, Mg, and Mn at the University of Toronto, Toronto, Ontario, with a Cameca SX-50 electron
105 microprobe at 20 kV and 30 nA with a ~ 1 μm beam. Data were processed using the Armstrong
106 (1988) matrix correction method and the CITZMU (Heinrich 1966; Henke and Ebisu 1974) mass

Revision 1

107 absorption coefficients database. In both EMP data sets, analyses with oxide totals not within
108 99.00-101.00% were rejected.

109 Prior to trace element analysis, linear regions of roughly uniform P content (see description of
110 zoning patterns in next section) were identified via element mapping using the scanning electron
111 microscope at the University of Toronto, at an accelerating voltage of 15 kV and with a
112 specimen current of ~6 nA. Trace elements were measured using laser ablation inductively
113 coupled plasma mass spectrometry (LA-ICP-MS) at the University of Toronto. A frequency
114 quintupled Nd:YAG laser coupled to a VG PQExcell quadrupole ICP-MS was operated at a
115 repetition rate of 10 Hz with a 18 μm spot size (intentionally small to avoid the ablation of
116 multiple regions differing in P content). For each analysis, 20 seconds of background collection
117 while flushing the ablation cell with He were followed by 60 seconds of data acquisition while
118 ablating a line in the sample. The NIST610 silicate glass standard was measured twice with a 55
119 μm spot before and after each set of 16 analyses, with Mn (measured using EMP as described
120 above) used as an internal reference element to correct for ablation yields in the standard. Data
121 were reduced using the GLITTER software package (version 4.4.4). A preliminary run included
122 a large suite of elements (Li, Na, Al, K, Ca, Sc, Ti, V, Cr, Co, Ni, Cu, Zn, Ga, Ge, As, Se, Rb, Sr,
123 Y, Zr, Nb, Mo, Ag, Cd, Sn, Te, Sb, Cs, La, Ce, Nd, Sm, Eu, Gd, Dy, Lu, Hf, Ta, W, Re, Au, Pb,
124 and Bi) but most were not detectable in the phosphoran olivine. In subsequent runs many
125 elements were eliminated from the analytical regime to increase the time spent counting on each
126 mass. Note that Na, K, Ca, and Ni may be present at ppm levels, given their concentrations in
127 Springwater P-free olivine reported by Hsu (2003) and Floss (2002), but these elements are
128 associated with high backgrounds in the NIST610 standard and therefore could not be detected in
129 this study. Analyses with >50 ppm Co were rejected because these elevated values likely reflect

Revision 1

130 contamination from the fine network of metal veining across the olivine grains (Springwater
131 metal contains 5880 ppm Co (Wasson and Choi 2003), whereas the olivine is reported at only 2-
132 7 ppm (Leitch et al. 1979)).

133

134

Distribution and textures

135 In the Springwater pallasite, phosphoran olivine occurs exclusively as epitaxial overgrowths on
136 the nominally P-free olivine crystals (Figure 1). A single region of phosphoran olivine identified
137 within the central portion of an olivine grain likely represents a grain edge sectioned by the
138 sample surface, based on concentric zoning similar to all other occurrences (described below).
139 Phosphoran overgrowths range from 28-459 μm in width and 130-4116 μm in length, or 137 x
140 1421 μm on average. Phosphoran olivine is ubiquitous in Springwater, with 47% of the P-free
141 olivine grains in the samples searched systematically bearing at least one overgrowth and 69
142 overgrowths observed in total. Phosphoran overgrowths occur on all three host olivine grain
143 boundary morphologies in Springwater: rounded (the majority of grains), subplanar and
144 complementary in shape to neighboring grains (described by Scott (1977) in the Brenham
145 pallasite), and jagged (occasionally present on small grains) (Figure 2). Phosphoran olivine is not
146 associated with any particular pallasitic phase other than its host olivine crystals, as the number
147 of overgrowths in contact with each other phase roughly mirrors their relative abundances at host
148 olivine grain boundaries (Figure 3a). Additionally, the phase in contact with phosphoran
149 overgrowths does not exert control over their size (Figure 3b).

150 Within phosphoran overgrowths, striking oscillatory zoning in P and Si is present on a fine (<10
151 μm) scale (Figure 4). Zones of uniform P content range from linear to serrate in shape, with both

Revision 1

152 morphologies often juxtaposed concentrically. Overgrowth regions proximal to the host grain are
153 generally more P-rich and more serrate than distal regions. The serrations are most readily
154 discernible in overgrowths imaged with EDS element mapping, but contrast adjustments to the
155 BSE images suggest that these zoning patterns are present within all overgrowths. The contact
156 between phosphoran and P-free olivine is always sharp, with no interruption to the macroscopic
157 contours of the host grain boundary where overgrowths occur (Figures 2 and 4). On the other
158 hand, overgrowth margins at the metal contact may be smooth but are more often irregular,
159 truncating the internal zoning (e.g. Figure 2a, inset). The olivine grains and their phosphoran
160 overgrowths are also cut by an irregularly branching network of ≤ 3 μm wide metal veins (Figure
161 2), a texture attributed to shock in meteorites (Stöffler et al. 1991).

162

163 **Geochemical analysis**

164 **Major and minor elements**

165 Springwater phosphoran olivine ranges from 2.07 to 7.13 wt% P_2O_5 (for full results from 179
166 EMP analyses, see online depository). The variable P_2O_5 content within single overgrowths and
167 sharp decrease to ~ 0 wt% at the contact to the host grain can be seen in traverses roughly
168 perpendicular to the grain boundary (Figure 5). The inverse relationship between P_2O_5 and SiO_2
169 content – and a similar correlation of half the magnitude between P_2O_5 and $\text{MgO}+\text{FeO}+\text{MnO}$ –
170 indicates the substitution of P for Si with vacancies in the octahedral site to balance charge
171 (Buseck and Clark 1984; Boesenberg and Hewins 2010). This substitution mechanism is
172 supported in the full data set by the slope of -0.52 with increasing P for $\text{Mg}+\text{Fe}+\text{Mn}$ cations (R^2
173 = 0.47), -1.01 for Si cations ($R^2 = 0.93$), and very nearly 0 for P+Si cations (Figure 6). As P is

Revision 1

174 incorporated into the structure, Fe and Mn appear to be preferentially excluded as compared with
175 Mg. The rate of Fe decrease with increasing P accounts for 34% of the total rate of divalent
176 cation decrease, while Fe occupies only 17% of the octahedral sites on average; similarly, the
177 rate of Mn decrease represents 1% of the total, though Mn occupies only 0.37% of the sites.
178 These discrepancies may be due to the greater size of octahedrally-coordinated Fe^{2+} (0.78 Å) and
179 Mn^{2+} (0.83 Å) as compared with Mg^{2+} (0.72 Å) (Henderson 1982).

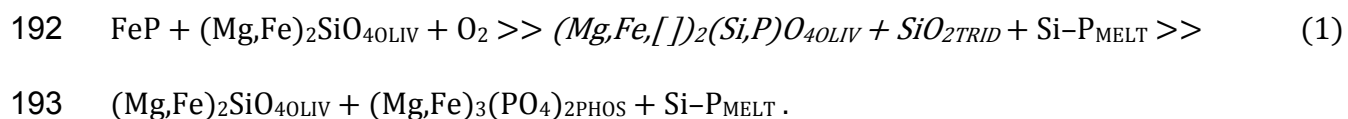
180 Trace elements

181 Full trace element data, including minimum detection limits, can be found in the online
182 depository. We tested the possibility of P accommodation in olivine through coupled substitutions
183 with 3+ cations (Milman-Barris et al. 2008) by plotting V and Cr concentrations against P levels
184 (Figure 7); Al could not be compared as it was not detectable above background. No relationship
185 exists between V and P_2O_5 or Cr and P_2O_5 ($R^2 = 0.01$ in both cases), suggesting this substitution
186 mechanism does not operate in the case of Springwater phosphoran olivine.

187

188 Discussion

189 Boesenberg and Hewins (2010) propose that phosphoran olivine crystallizes via the following
190 pathway at $\sim 1000^\circ\text{C}$, an oxygen fugacity of IW-1, and 0.1 MPa (italics indicate metastable
191 intermediates):



Revision 1

194 Though pallasites almost certainly resided at pressures greater than 0.1 MPa because of their
195 burial depth (Yang et al. 2010), Springwater olivine has been estimated at $fO_2 \sim IW$ (Righter et al.
196 1990). Assuming a reaction sequence in Springwater similar to equation (1), the reduced stability
197 of schreibersite during cooling (Buseck and Holdsworth 1977; Olsen and Frederiksson 1966)
198 could have caused P enrichment in a residual silicate melt surrounding the olivine crystals, the
199 persistence of which has been postulated as a necessary condition for creating the rounded grain
200 boundaries (Ohtani 1983; Boesenberg et al. 2012). Crystallization of the phosphoran olivine
201 from a melt, as opposed to via replacement reactions below the solidus (Buseck 1977), is
202 strongly supported by the concentric P zoning and sharp contacts to the uninterrupted contours of
203 host grains. The metastable character of the phosphoran overgrowths is corroborated by irregular
204 outer margins that cross-cut the P zoning in a manner suggestive of dissolution (e.g. Figure 2a,
205 inset). Though farringtonite ($Mg_3(PO_4)_2$) is an end product of this reaction sequence as proposed
206 by Boesenberg and Hewins (2010), the vast majority of Springwater farringtonite likely derives
207 from other sources because it is not spatially correlated with phosphoran olivine – and moreover,
208 a mass balance problem is apparent in the orders of magnitude greater volume of farringtonite
209 (e.g. Figure 1a) than that of any conceivable original extent of phosphoran overgrowths.

210 The dramatic compositional zoning we observe within Springwater's phosphoran olivine begs a
211 more sophisticated discussion of its formation mechanisms. Oscillatory zoning in P at trace
212 levels is common in igneous olivine, though the mechanisms that produce these features are not
213 fully understood (Milman-Barris et al. 2008). Although zoning of this nature can develop due to
214 wildly fluctuating P concentrations in the melt, we rule out such a scenario without any plausible
215 mechanism that might account for repeated melt influx to the Springwater pallasitic region.
216 Furthermore, Cr and V systematics of individual overgrowths appear to reflect simple fractional

Revision 1

217 crystallization trends from closed melt reservoirs (Figure 8). Under such conditions, Cr/V would
218 be expected to rise with increasing Cr because olivine/melt partition coefficients at ~IW are ~0.6
219 for Cr (Gaetani and Grove 1997) and ~0.5 for V (Mallmann and O'Neill 2009). Despite the
220 structural changes predicted when significant P₂O₅ is incorporated into olivine (Boesenberg and
221 Hewins 2010), the presence of highly linear trends in Cr/V versus Cr in the predicted direction
222 suggests that relative partitioning of Cr and V in Springwater phosphoran olivine is broadly
223 similar to that expected for olivine with little or no P. Given this evidence for formation of
224 phosphoran overgrowths from closed melt pockets, we offer two alternative interpretations of the
225 oscillatory zoning that rest on the more plausible premise of changing crystallization rate.

226 Possibly, periods of rapid crystal growth allow greater incorporation of incompatible P cations
227 but also deplete the adjacent melt layer of the major elements that form olivine, thereby causing
228 intervals of slower crystallization of olivine poorer in P (Milman-Barris et al. 2008). Modeling
229 by Watson and Müller (2009) demonstrates disequilibrium uptake of incompatible elements
230 where crystallization occurs more quickly than cations are able to diffuse away through the
231 boundary layer of melt. If this process operated in Springwater, the overgrowth zones highest in
232 P (indicating the most rapid crystallization) might be expected to show enrichment in other
233 incompatible elements also limited by diffusivity in the melt. However, no strongly incompatible
234 trace elements are detectable in Springwater phosphoran olivine, making it difficult to evaluate
235 this hypothesis. It is also challenging to assess the rate of P diffusion in the melt because many of
236 the variables known to control diffusivity, such as temperature, pressure, and melt composition
237 (Hofmann 1980), are not well constrained.

238 On the other hand, the fine-scale zoning in P may be related not to limitations on diffusion
239 through the melt, but rather to unique properties of P within the actively forming crystal lattice.

Revision 1

240 The structural differences of a newly formed lattice layer as compared to the inner lattice are
241 often associated with higher equilibrium cation concentrations, thus allowing “growth
242 entrapment” of normally incompatible constituents when additions to the lattice are rapid enough
243 (Watson and Liang 1995). During the crystallization of the Springwater phosphoran olivine
244 overgrowths, more frequent lattice additions may have produced zones richer in P while periods
245 of slower growth may have allowed each layer more time to transition toward the lower-P
246 equilibrium concentration of the inner lattice. The absence of correlated Cr or V enrichments
247 with P may simply reflect “normal” equilibrium partitioning behavior for these elements even in
248 the outer lattice.

249 The unusual serrate morphology of the P zoning is also a likely consequence of growth rate. The
250 most similar pattern reported in the literature is “fir tree zoning” in calcite cements, thought to
251 develop through abrupt changes in the relative growth rate of adjacent crystal sectors (Raven and
252 Dickson 1989); however, it is unlikely the pattern is crystallographically controlled in
253 Springwater. Not only are serrations interspersed laterally on single crystal faces, rather than
254 forming stacked triangles along sector boundaries as in fir tree zoning, but also serrate, linear,
255 and intermediate forms are often observed within single overgrowths. Because serrate zones tend
256 to predominate close to the host grain interface, and often are the most phosphorus-rich, these
257 patterns may be a record of high-density crystal nucleation and rapid growth due to significant
258 undercooling (Swanson 1977). A net decrease in the rate of crystallization (superimposed on the
259 smaller-scale rate oscillations) may have produced increasingly linear and P-poor layers as the
260 overgrowths advanced outwards.

261 Combined with the evidence for rapid crystallization from a melt, textural relationships can be
262 used to bracket the relative timing of phosphoran olivine formation. Not only do the phosphoran

Revision 1

263 overgrowths overprint the rounding of host grain margins, but they also post-date the opening of
264 linear interstices between adjacent well-annealed olivine crystals, as well as the formation of
265 isolated fragmental grains. The latest possible time of phosphoran olivine formation is
266 constrained by the cross-cutting metal shock veins, which in turn must have been generated
267 before Springwater cooled below 360°C considering the preserved paleomagnetic signature in
268 pallasitic metal (Tarduno et al. 2012; Bryson et al. 2015). It is probable that phosphoran olivine
269 formed far earlier than this, in fact, since the uninterrupted contours of host olivine grain
270 boundaries indicate overgrowth crystallization from the original residual melt that facilitated
271 macroscopic grain rounding (Ohtani 1983; Boesenberg et al. 2012) rather than from any melt
272 formed subsequent to initial cooling below the solidus. Phosphoran olivine thus likely
273 crystallized prior to the long slow cooling period inferred from the delicate Widmanstätten
274 texture (Owen and Burns 1939) and Ni diffusion profiles (Yang et al. 2010) within the metal
275 phases.

276

277

Implications

278 The macroscopic rounding of the olivine grains is taken as evidence that Springwater
279 experienced at least 10-100 m.y. above ~1250°C (Scott 1977; Saiki et al. 2003). Below ~700°C,
280 Main Group pallasites are estimated to have cooled at 2.5-18°C/m.y (5.1±0.7°C/m.y for
281 Springwater; Yang et al. 2010). What event could have occurred between these extended periods
282 of near-stasis in the local environment to trigger the episode of extremely rapid crystallization
283 necessary to crystallize and preserve phosphoran olivine? One possible mechanism for
284 interrupting the gradual cooling trajectory is an impact to the parent body. Either substantial

Revision 1

285 surface excavation or the generation of impact melt (thus initiating a convective cooling regime)
286 could dramatically accelerate the cooling of the pallasitic region. Reaccretion of the disrupted
287 material and/or the shift back to a conductive cooling regime after melt solidification may have
288 facilitated the transition back to the low cooling rates recorded by the metal phases; the
289 dissolution of outer margins of phosphoran overgrowths implies that cooling rates began to
290 decrease even before temperatures had fallen significantly below the solidus.

291 An impact to the Main Group pallasite parent body that brought temperatures too low for the
292 efficient rounding of olivine grains is independently indicated by Springwater's pervasive slight
293 partings between grains whose contours imply annealing in contact with olivine rather than
294 metal. While the grains with mutual boundaries are generally aligned according to their [100]
295 axes, the slightly separated grains are more misaligned but still definitively non-random,
296 suggesting that these latter grains broke apart from clusters after cooling had proceeded too far
297 for their complementary-shaped boundaries to become rounded (Fowler-Gerace et al. in prep.).
298 The isolated fragmental grains lend additional support for an impact subsequent to cooling below
299 $\sim 1250^{\circ}\text{C}$. The overprinting phosphoran overgrowths may have crystallized immediately
300 following the event responsible for these olivine textural modifications, although the
301 observations do not exclude their formation after another later impact.

302 Alternatively, the formation of phosphoran olivine overgrowths could be explained by viscous
303 entrainment of olivine clusters in convection currents within the molten metal of the pallasitic
304 region, perhaps causing multiple cycles of crystallization and dissolution as host olivine grains
305 were repeatedly transported through a temperature range just straddling the solidus. Viscous
306 entrainment is possible when the viscous forces are greater than the buoyancy forces. Simple
307 calculations with reasonable estimates of the relevant parameters for Springwater reveal that the

Revision 1

308 metal must convect at a velocity greater than 1 m/s in order to entrain olivine. Using convection
309 scaling laws from Carrigan (1987), we estimate that the upper bound for flow velocity in a
310 convecting pallasitic region 300 m to 30 km in size (the highest value chosen as the difference in
311 estimated burial depth between the Esquel and Imilac pallasites; Tarduno et al. 2012) would be
312 0.28 to 2.3 m/s, respectively. Entrainment of olivine into the convective flow is therefore only
313 possible with a large unified body of molten metal; whether transport of olivine grains across this
314 distance would also yield a temperature differential conducive to cycles of crystallization and
315 only partial dissolution of the metastable phosphoran overgrowths is unknown.

316 However, such a scenario may not explain the presence of phosphoran overgrowths on the
317 fragmental olivine of the Brahin pallasite (Buseck 1977). It is difficult to imagine that olivine
318 grains entrained within molten metal convecting faster than 1 m/s would not become rounded
319 through mutual collisions over millions of years (the assumed duration in the absence of impact-
320 related modification of the slow cooling trajectory reported by Yang et al. (2010)). Additionally,
321 the suggested convection mechanism may be incongruous with the serrate shapes of only the
322 earliest growth zones of Springwater's phosphoran olivine. One would expect the degree of
323 undercooling to be roughly the same each time olivine clusters were carried to shallower depths,
324 therefore promoting high-density nucleation for all generations of phosphoran olivine. A
325 suddenly accelerated cooling rate due to impact, on the other hand, may be more consistent with
326 the zoning features suggestive of one crystal nucleation event during extremely rapid initial
327 growth, followed by generally slowing crystallization and smaller rate oscillations due to
328 boundary layer effects (Watson and Müller 2009) or growth entrapment (Watson and Liang
329 1995).

Revision 1

330 Multiple impacts to the Main Group pallasite parent body subsequent to its differentiation but
331 prior to solidification of the pallasitic metal is not implausible. Using the present-day impact
332 probability per year on Earth modeled by Le Feuvre and Wieczorek (2011), the probability of
333 impact P by bodies with radius r over time t to the Main Group pallasite parent body can be
334 estimated to an order of magnitude by

$$335 \quad P(r, t) \approx 10^{-8} \left(\frac{r}{5\text{km}} \right)^{-13/5} \left(\frac{R}{R_E} \right)^2 \left[\frac{(2GR^2\rho/V^2)+1}{(2GR_E^2\rho_E/V_E^2)+1} \right] \left(\frac{a_{\text{Pallasite}}}{1\text{AU}} \right)^2 \left(\frac{f(t)}{10^{10}\text{g/yr}} \right) \quad (2)$$

336 where R is the radius of the target body, G is the universal gravitational constant, ρ is the bulk
337 density of the body, V is the orbital velocity, a is the heliocentric distance, $f(t)$ is the terrestrial
338 impact mass flux as a function of time (Koeberl 2006), and the subscript E denotes values for
339 Earth. Figure 9 shows the impactor flux, assuming 200 km radius for the Main Group pallasite
340 parent body (Tarduno et al. 2012), heliocentric distance approximated by the asteroid belt, and
341 average density 3.5 g/cc. Before Springwater cooled through 360°C (after which reheating is
342 impossible owing to the preservation of a coherent paleomagnetic signature; Bryson et al. 2015),
343 tens of 10 km-radius impactors and orders of magnitude more smaller impactors are predicted to
344 have encountered the parent body.

345 The textural relationships among phosphoran olivine, host olivine grains, and metal in
346 Springwater imply up to two late impacts to the Main Group pallasite parent body, besides the
347 impact proposed to have initially integrated metal into the olivine-rich upper mantle region
348 (Tarduno et al. 2012). One additional impact may have induced the breakup of olivine clusters
349 and accelerated cooling rates substantially, preventing the efficient rounding of olivine margins
350 exposed to metal as well as promoting the rapid crystallization and preservation of phosphoran
351 overgrowths. A second impact associated with temperatures below the olivine solidus (~1320°C

Revision 1

352 at the eutectic with farringtonite (Boesenberg and Hewins 2010)) but above that of the metal
353 matrix (~950°C based on ~12.7% each Ni and S as in Springwater (Buseck 1977; Starykh and
354 Sineva 2012)) could have fractured olivine grains and their overgrowths, creating space that
355 would naturally fill with molten metal. The absence of phosphoran olivine in the majority of
356 Main Group pallasites may be related to lower local P concentrations or simply a lack of
357 detection by previous investigators.

358

359

Acknowledgements

360 The authors would like to acknowledge the Louise Hawley Stone acquisition grant and Canadian
361 Cultural Property Export and Review board funding for the purchase of the Springwater pallasite
362 sample, Ian Nicklin (Royal Ontario Museum) for facilitating sample preparation, Brian Joy
363 (Queen's University) and Yanan Liu (University of Toronto) for assistance with electron
364 microprobe analyses, Colin Bray (University of Toronto) for aid in LA-ICP-MS data acquisition,
365 James Brenan for advice regarding trace element data collection and interpretation of results, and
366 Bob Tian for aid in modeling impactor flux to the Main Group pallasite parent body. Funding for
367 the research was from a NSERC Discovery Grant (to KTT), a peer review grant from the Louise
368 Hawley Stone Trust, the Canadian Space Agency Astromaterials Training and Research
369 Opportunities (ASTRO) Graduate Student Incentive Award, and the University of Toronto
370 Connaught Scholarship.

371

372

References

Revision 1

- 373 Agrell, S.O., Charnley, N.R., and Chinner, G.A. (1998) Phosphoran olivine from Pine Canyon,
374 Piute Co., Utah. *Mineralogical Magazine*, 62, 265-269.
- 375 Anderson, A.T., and Greenland, L.P. (1969) Phosphorus fractionation diagram as a quantitative
376 indicator of crystallization differentiation of basaltic liquids. *Geochimica et*
377 *Cosmochimica Acta*, 33, 493-505.
- 378 Armstrong, J.T. (1988) Quantitative analysis of silicate and oxide minerals: comparison of
379 Monte Carlo, ZAF and phi-rho-z procedures. *Microbeam Analysis*, 23, 239-246.
- 380 Boesenberg, J.S. (2006) Wrought iron from the *USS Monitor*: Mineralogy, petrology, and
381 metallography. *Archaeometry*, 48, 613-631.
- 382 Boesenberg, J.S., and Hewins, R.H. (2010) An experimental investigation into the metastable
383 formation of phosphoran olivine and pyroxene. *Geochimica et Cosmochimica Acta*, 74,
384 1923-1941.
- 385 Boesenberg, J.S., Delaney, J.S., and Hewins, R.H. (2012) A petrological and chemical
386 reexamination of Main Group pallasite formation. *Geochimica et Cosmochimica Acta*,
387 89, 134-158.
- 388 Brunet, F., and Chazot, G. (2001) Partitioning of phosphorus between olivine, clinopyroxene and
389 silicate glass in a spinel lherzolite xenolith from Yemen. *Chemical Geology*, 176, 51-72.
- 390 Bryson, J.F.J., Nichols, C.I.O, Herrero-Albillos, J., Kronast, F., Kasama, T., Alimadadi, H., van
391 der Laan, G., Nimmo, F., and Harrison, R.J. (2015) Long-lived magnetism from
392 solidification-driven convection on the pallasite parent body. *Nature*, 517, 472-475.

Revision 1

- 393 Buseck, P.R. (1977) Pallasite meteorites – Mineralogy, petrology and geochemistry. *Geochimica*
394 *et Cosmochimica Acta*, 41, 711-740.
- 395 Buseck, P.R., and Holdsworth, E. (1977) Phosphate minerals in pallasite meteorites.
396 *Mineralogical Magazine*, 41, 91-102.
- 397 Buseck, P.R., and Clark, J. (1984) Zaisho – A pallasite containing pyroxene and phosphoran
398 olivine. *Mineralogical Magazine*, 48, 229-235.
- 399 Carrigan, C.R. (1987) The magmatic Rayleigh number and time dependent convection in cooling
400 lava lakes. *Geophysical Research Letters*, 14, 915-918.
- 401 Floss, C. (2002) Queen Alexandra Range 93148: A new type of pyroxene pallasite? *Meteoritics*
402 *& Planetary Science*, 37, 1129-1139.
- 403 Gaetani, G.A., and Grove, T.L. (1997) Partitioning of moderately siderophile elements among
404 olivine, silicate melt, and sulfide melt: Constraints on core formation in the Earth and
405 Mars. *Geochimica et Cosmochimica Acta*, 61, 1829-1846.
- 406 Goodrich, C.A. (1984) Phosphoran pyroxene and olivine in silicate inclusions in natural iron-
407 carbon alloy, Disko Island, Greenland. *Geochimica et Cosmochimica Acta*, 48, 2769-
408 2771.
- 409 Goodrich, C.A. (2003) Petrogenesis of olivine-phyric shergottites Sayh al Uhaymir 005 and
410 Elephant Moraine A79001 lithology A. *Geochimica et Cosmochimica Acta*, 67, 3735-
411 3772.

Revision 1

- 412 Heinrich, K.F.J. (1966) X-ray absorption uncertainty. In T.D. McKinley, K.F.J. Heinrich, and
413 D.B. Wittry, Eds., *The Electron Microprobe*, p. 296-377. John Wiley and Sons, New
414 York.
- 415 Heinrich, K.F.J. (1986) Mass absorption coefficients for electron probe microanalysis. In J.B.
416 Brown and R.H. Packwood, Eds., *Proceedings of the 11th international congress on X-*
417 *ray optics and microanalysis*, p. 67-119. London, Canada.
- 418 Henderson, P., Ed. (1982) *Structural Controls of Element Distribution*. In *Inorganic*
419 *Geochemistry*, p. 102-155. Pergamon, Oxford.
- 420 Henke, B.L., and Ebisu, E.S. (1974) Low energy x-ray and electron absorption within solids
421 (100–1500 eV region). In C.L. Grant, C.S. Barrett, J.B. Newkirk, and C.O. Ruud, Eds.,
422 *Advances in X-Ray Analysis*, 17, p. 150-213. Plenum, New York.
- 423 Hofmann, A.W. (1980) Diffusion in natural silicate melts: A critical review. In R.B. Hargraves,
424 Ed., *Physics of Magmatic Processes*, p. 385-418. Princeton University Press, New Jersey.
- 425 Hsu, W. (2003) Minor element zoning and trace element geochemistry of pallasites. *Meteoritics*
426 *& Planetary Science*, 38, 1217-1241.
- 427 Koeberl, C. (2006) The record of impact processes on the early Earth: A review of the first 2.5
428 billion years. In Reimold, W.U., and Gibson, R.L., Eds., *Processes on the Early Earth:*
429 *Geological Society of America Special Paper 405*, p. 1-22.
- 430 Le Feuvre, M., and Wieczorek, M.A. (2011) Nonuniform cratering of the Moon and a revised
431 crater chronology of the inner Solar System. *Icarus*, 214, 1-20.

Revision 1

- 432 Leitch, C.A., Steele, I.M., Hutcheon, I.D., and Smith, J.V. (1979) Minor elements in pallasites:
433 Zoning in Springwater olivine. Lunar and Planetary Science Conference, 10, 716-718.
- 434 Mallmann, G., and O'Neill, H.S.C. (2009) The crystal/melt partitioning of V during mantle
435 melting as a function of oxygen fugacity compared with some other elements (Al, P, Ca,
436 Sc, Ti, Cr, Fe, Ga, Y, Zr and Nb). *Journal of Petrology*, 50, 1765-1794.
- 437 Mallmann, G., O'Neill, H.S.C., and Klemme, S. (2009) Heterogeneous distribution of
438 phosphorus in olivine from otherwise well-equilibrated spinel peridotite xenoliths and its
439 implications for the mantle geochemistry of lithium. *Contributions to Mineralogy and
440 Petrology*, 158, 485-504.
- 441 McKibbin, S.J., O'Neill, H.S.C., Mallmann, G., and Halfpenny, A. (2013) LA-ICP-MS mapping
442 of olivine from the Brahin and Brenham meteorites: Complex elemental distributions in
443 the pallasite olivine precursor. *Geochimica et Cosmochimica Acta*, 119, 1-17.
- 444 Milman-Barris, M.S., Beckett, J.R., Baker, M.B., Hofmann, A.E., Morgan, Z., Crowley, M.R.,
445 Vielzeuf, D., and Stolper, E. (2008) Zoning of phosphorus in igneous olivine.
446 *Contributions to Mineralogy and Petrology*, 155, 739-765.
- 447 Ohtani, E. (1983) Formation of olivine textures in pallasites and thermal history of pallasites in
448 their parent body. *Physics of the Earth and Planetary Interiors*, 32, 182-192.
- 449 Olsen, E., and Fredriksson, K. (1966) Phosphates in iron and pallasite meteorites. *Geochimica et
450 Cosmochimica Acta*, 30, 459-470.

Revision 1

- 451 Owen, E.A., and Burns, B.D. (1939) X-ray study of some meteoric irons. The Philosophical
452 Magazine, 28, 497-512.
- 453 Pouchou, J.L., and Pichoir, F. (1985) PAP (phi-rho-Z) procedure for improved quantitative
454 microanalysis. In J.T. Armstrong, Ed., Microbeam Analysis, p. 104-106. San Francisco
455 Press, San Francisco.
- 456 Raven, M.J., and Dickson, J. (1989) Fir-tree zoning – An indicator of pulsed crystallization in
457 calcite cement crystals. Sedimentary Geology, 65, 249-259.
- 458 Righter, K., Arculus, R.J., Delano, J.W., and Paslick, C. (1990) Electrochemical measurements
459 and thermodynamic calculations of redox equilibria in pallasite meteorites: Implications
460 for the eucrite parent body. Geochimica et Cosmochimica Acta, 54, 1803-1815.
- 461 Saiki, K., Laporte, D., Vielzeuf, D., Nakashima, S., and Boivin, P. (2003) Morphological
462 analysis of olivine grains annealed in an iron-nickel matrix: experimental constraints on
463 the origin of pallasites and on the thermal history of their parent bodies. Meteoritics &
464 Planetary Science, 38, 427-444.
- 465 Scott, E.R.D. (1977). Formation of olivine-metal textures in pallasite meteorites. Geochimica et
466 Cosmochimica Acta, 41, 693-710.
- 467 Sonzogni, Y., Devouard, B., Provost, A., and Devidal, J.-L. (2009) Olivine-hosted melt
468 inclusions in the Brahin pallasite. In Meteoritics and Planetary Science Supplement, p.
469 5070, 72nd Annual Meeting of the Meteoritical Society, Nancy, France.

Revision 1

- 470 Spandler, C., and O'Neill, H.S.C. (2009) Diffusion and partition coefficients of minor and trace
471 elements in San Carlos olivine at 1,300°C with some geochemical implications.
472 Contributions to Mineralogy and Petrology, 159, 791-818.
- 473 Starykh, R.V., and Sineva, S.I. (2012) Study of the liquidus and solidus surfaces of the
474 quaternary Fe–Ni–Cu–S system: V. Refinement and addition of the data on the ternary
475 Fe–Ni–S and Fe–Ni–Cu phase diagrams. Russian Metallurgy, 3, 189-194.
- 476 Stöffler, D., Keil, K., and Scott, E.R.D. (1991) Shock metamorphism of ordinary chondrites.
477 Geochimica et Cosmochimica Acta, 55, 3845-3867.
- 478 Swanson, S.E. (1977) Relation of nucleation and crystal-growth rate to the development of
479 granitic textures. American Mineralogist, 62, 966-978.
- 480 Tarduno, J.A., Cottrell, R.D., Nimmo, F., Hopkins, J., Voronov, J., Erickson, A., Blackman, E.,
481 Scott, E.R.D., and Robert McKinley, R. (2012) Evidence for a dynamo in the main group
482 pallasite parent body. Science, 338, 939-942.
- 483 Tarduno, J.A., and Cottrell, R.D. (2013) Paleomagnetism of the Springwater pallasite: Further
484 evidence for a dynamo in the Main Group pallasite parent body. 44th Lunar and Planetary
485 Science Conference, Texas.
- 486 Tropper, P., Recheis, A., and Konzett, J. (2004) Pyrometamorphic formation of phosphorus-rich
487 olivines in partially molten metapelitic gneisses from a prehistoric sacrificial burning site
488 (Ötz Valley, Tyrol, Austria). European Journal of Mineralogy, 16, 631-640.

Revision 1

- 489 Wadhwa, M., Srinivanson, G., Carlson, R.W. (2006) Timescales of planetesimal differentiation
490 in the early solar system. *Meteoritics and the Early Solar System II*, 715-731.
- 491 Wang, Y., Hua, X., and Hsu, W. (2007) Petrogenesis of opaque assemblages in the Ningqiang
492 carbonaceous chondrite. *Science in China Series D: Earth Sciences*, 50, 886-896.
- 493 Wasson, J.T., Lange, D.E., and Francis, C.A. (1999) Massive chromite in the Brenham pallasite
494 and the fractionation of Cr during the crystallization of asteroidal cores. *Geochimica et*
495 *Cosmochimica Acta*, 63, 1219-1232.
- 496 Wasson, J.T., and Choi, B.G. (2003) Main-group pallasites: Chemical composition, relationship
497 to IIIAB irons, and origin. *Geochimica et Cosmochimica Acta*, 67, 3079-3096.
- 498 Watson, E.B., and Liang, Y. (1995) A simple model for sector zoning in slowly grown crystals:
499 implications for growth rate and lattice diffusion, with emphasis on accessory minerals in
500 crustal rocks. *American Mineralogist*, 80, 1179-1187.
- 501 Watson, E.B., and Müller, T. (2009) Non-equilibrium isotopic and elemental fractionation during
502 diffusion-controlled crystal growth under static and dynamic conditions. *Chemical*
503 *Geology*, 267, 111-124.
- 504 Yang, J., Goldstein, J.I., and Scott, E.R.D. (2010) Main-group pallasites: Thermal history,
505 relationship to IIIAB irons, and origin. *Geochimica et Cosmochimica Acta*, 74, 4471-
506 4492.
- 507
- 508

Revision 1

509

510

Revision 1

511

Figure Captions

512 **Figure 1.** (BSE images) Springwater contains abundant phosphoran olivine (shaded in red and
513 indicated by yellow ellipses) as partial overgrowths on the large olivine grains. Overgrowths are
514 randomly distributed, irrespective of spatial variations in accessory mineralogy: compare large
515 clots of farringtonite in matrix of **(a)** with predominantly metal matrix of **(b)**. Phases indicated are
516 olivine (ol), taenite and kamacite (Fe-Ni), farringtonite (far), troilite (tro), stanfieldite (sta), and
517 schreibersite (scb). Locations marked (2a), (2b), and (2c) correspond to Figure 2.

518 **Figure 2.** (BSE images) Phosphoran overgrowths are observed on a variety of host grain
519 margins, including **(a)** rounded, **(b)** planar/complementary, and **(c)** fragmental. Insets at right are
520 enlarged portions with contrast exaggerated to show contact between phosphoran and P-free
521 olivine (indicated with arrows); regions richer in P appear darker.

522 **Figure 3.** **(a)** Percent of overgrowths observed in contact with farringtonite, stanfieldite, metal,
523 troilite, and schreibersite, as compared with the expected profile assuming a random distribution
524 of overgrowths (based on the estimated relative abundances of each phase at host olivine grain
525 margins). **(b)** Mean area (approximated by the maximum width of an overgrowth multiplied by
526 its length along the host grain boundary) of overgrowths observed in contact with each phase,
527 normalized to the area of the largest overgrowth (uncertainties shown are standard errors of the
528 mean).

529 **Figure 4.** **(a)** BSE image of a typical phosphoran overgrowth. Fine-scale oscillatory zoning in
530 linear and serrate patterns is revealed through WDS maps for **(b)** P K \square and **(c)** Si K \square .

Revision 1

531 **Figure 5.** EMP analyses across three phosphoran overgrowths (different colors) show correlated
532 variations in P_2O_5 , SiO_2 , and $MgO+FeO+MnO$ with distance (normalized to total width of
533 overgrowth) and an abrupt transition to the nearly P-free composition of the host olivine crystal
534 (all symbols are larger than 1σ error based on counting statistics).

535 **Figure 6.** Data from 179 EMP analyses in phosphoran olivine show consistent relationships
536 between P, Si, and octahedral site cations (all symbols are larger than 1σ error based on counting
537 statistics).

538 **Figure 7.** Cr and V concentrations (uncertainties are 1σ error based on counting statistics) versus
539 P_2O_5 (uncertainties are half the difference between the EMP analyses at each end of laser
540 ablation line, plus 1σ error based on counting statistics), with analyses from single overgrowths
541 shown as the same color.

542 **Figure 8.** Cr/V versus Cr concentration, with analyses from single overgrowths shown as the
543 same color (1σ error based on counting statistics shown). Arrow indicates rough approximation
544 of the trend expected during fractional crystallization from a closed melt reservoir, given slightly
545 higher compatibility of Cr than V in olivine.

546 **Figure 9.** Number of impactors per 100 m.y. **(a)** and cumulative number of impacts **(b)** expected
547 to occur on a 200-km radius planetesimal in the asteroid belt as a function of time, with different
548 possible impactor radii indicated. Core-mantle differentiation of planetesimals is thought to have
549 occurred within 10 m.y. of solar system formation (Wadhwa et al. 2006), so 4.5 Ga can be taken
550 as a conservative estimate of the latest time the upper mantle region differentiated to nearly
551 monomineralic olivine cumulates. The latest possible time that impacts could account for the
552 textures we observe in Springwater is shown with a dashed line indicating the approximate time

Revision 1

553 that Springwater cooled below 360°C (~180 m.y. after accretion, assuming 40 km burial depth;
554 Tarduno and Cottrell 2013) and began to preserve a paleomagnetic signature within the
555 tetraenaite cloudy zone (Bryson et al. 2015).

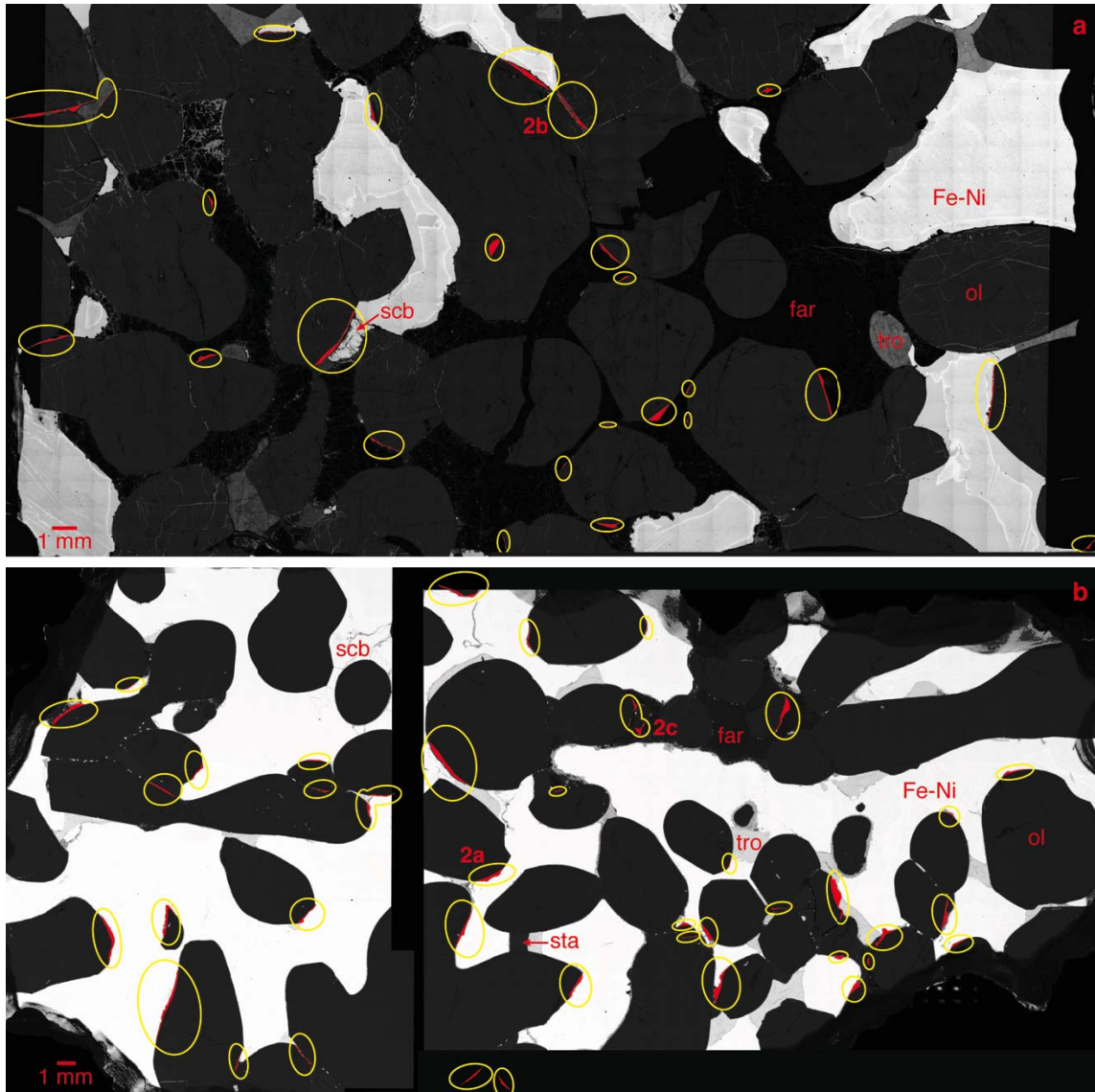
556

557

Revision 1

558

Figures

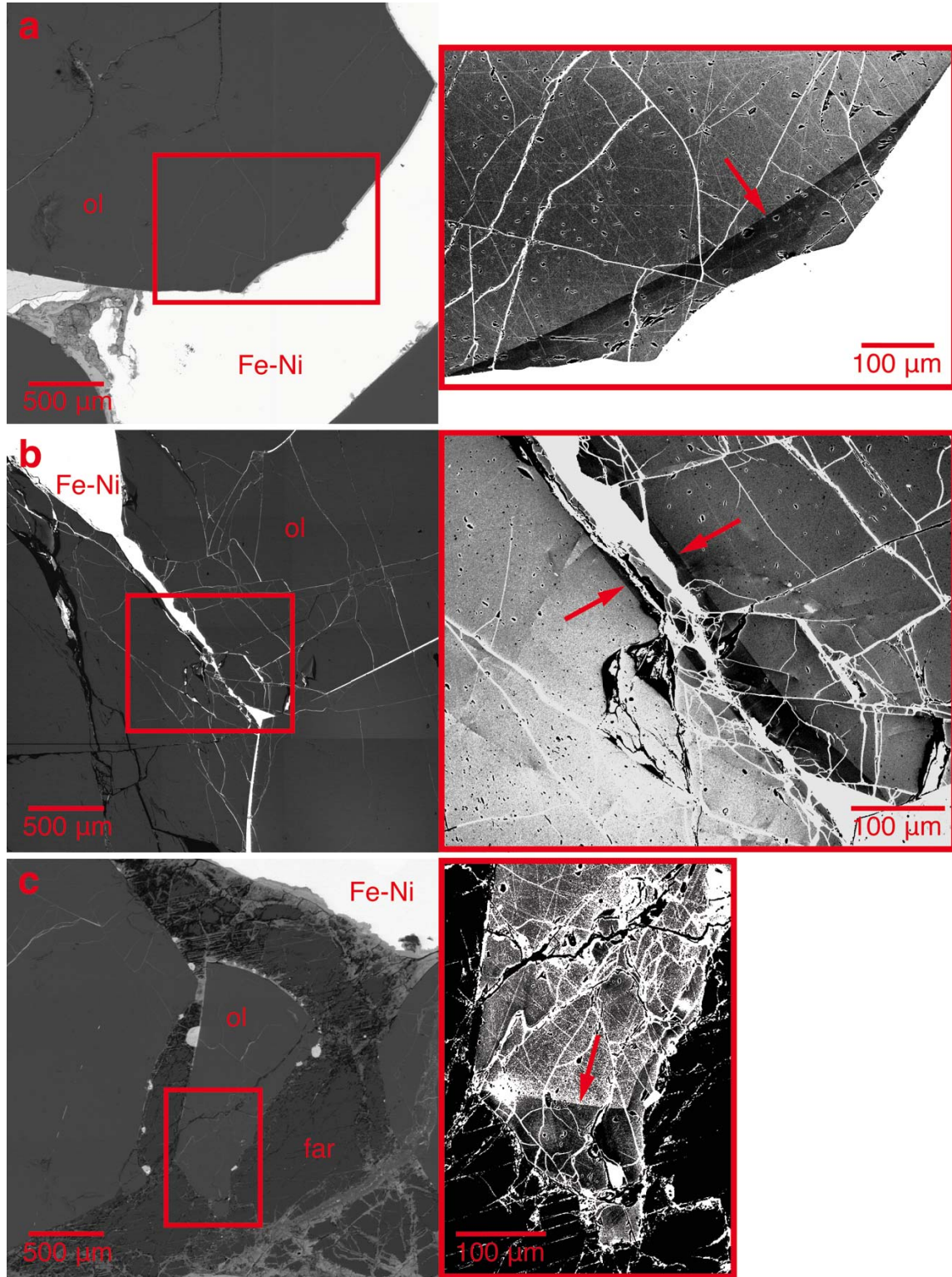


559

560 **Figure 1.**

561

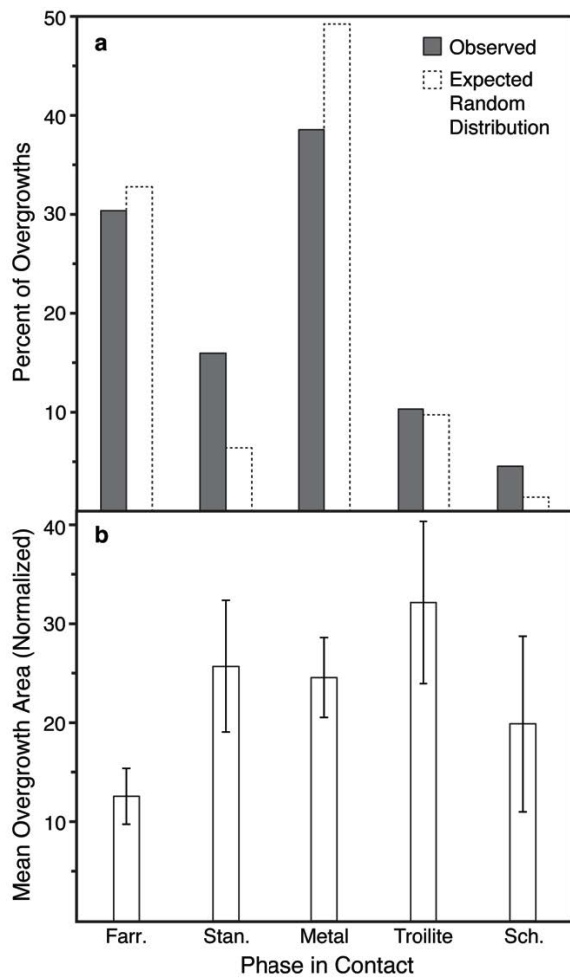
Revision 1



562

563 **Figure 2.**

Revision 1

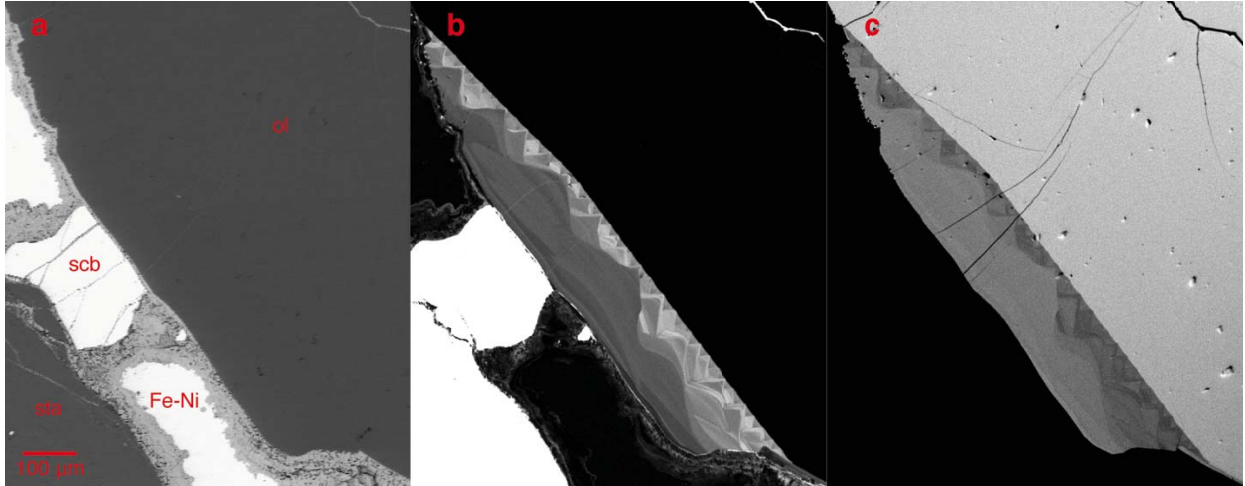


564

565 **Figure 3.**

566

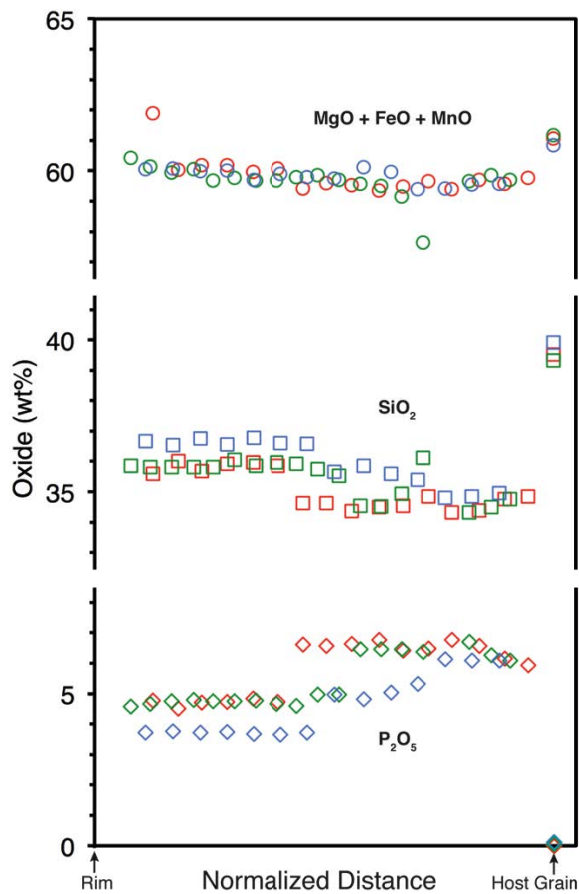
Revision 1



567

568 **Figure 4.**

Revision 1

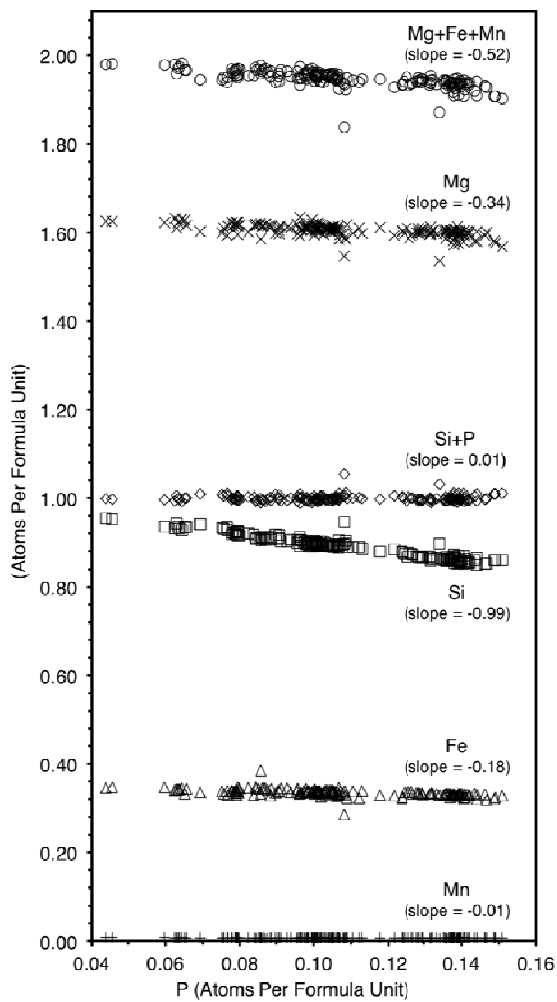


569

570 **Figure 5.**

571

Revision 1

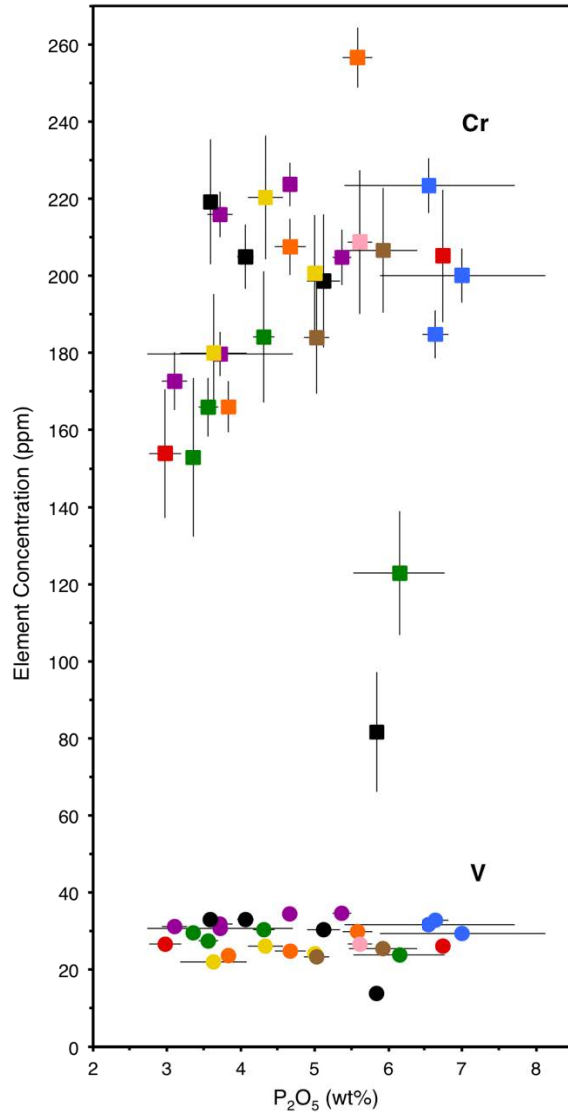


572

573 **Figure 6.**

574

Revision 1

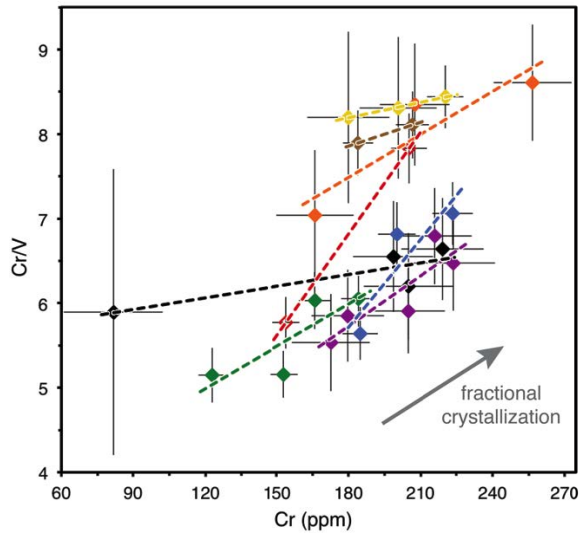


575

576 **Figure 7.**

577

Revision 1

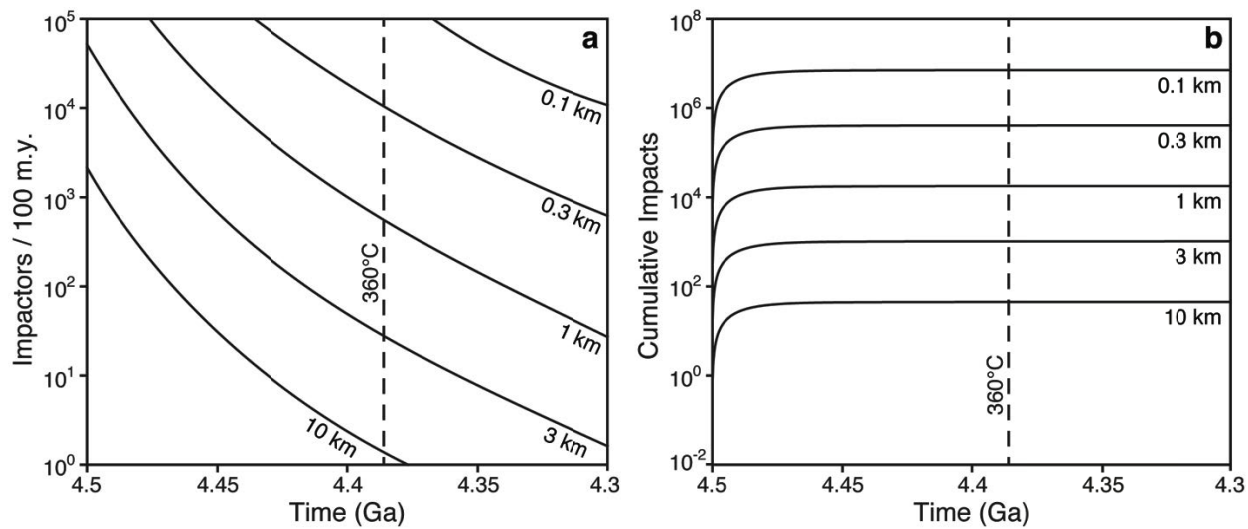


578

579 **Figure 8.**

580

Revision 1



581

582 **Figure 9.**